2012

High Performance Modeling of Atmospheric Re-Entry Vehicles

Alexandre Martin
University of Kentucky, alexandre.martin@uky.edu

Leonardo C. Scalabrin
Embraer S.A., Brazil

Iain D. Boyd
University of Michigan

High performance modeling of atmospheric re-entry vehicles

Journal of Physics: Conference Series **341** (2012) 012002 doi:10.1088/1742-6596/341/1/012002

High performance modeling of atmospheric re-entry vehicles

Alexandre Martin[1], Leonardo C. Scalabrin[2] and Iain D. Boyd[3]

[1] Department of Mechanical Engineering, University of Kentucky, Lexington, KY, 40506, USA
[2] Embraer S.A., São José dos Campos, 12243-000, Brazil
[3] Department of Aerospace Engineering, University of Michigan, Ann Arbor, MI, 48109, USA

E-mail: alexandre.martin@uky.edu, leonardo.scalabrin@embraer.com.br, iainboyd@umich.edu

Abstract. Re-entry vehicles designed for space exploration are usually equipped with thermal protection systems made of ablative material. In order to properly model and predict the aerothermal environment of the vehicle, it is imperative to account for the gases produced by ablation processes. In the case of charring ablators, where an inner resin is pyrolyzed at a relatively low temperature, the composition of the gas expelled into the boundary layer is complex and may lead to thermal chemical reactions that cannot be captured with simple flow chemistry models. In order to obtain better predictions, an appropriate gas flow chemistry model needs to be included in the CFD calculations. Using a recently developed chemistry model for ablating carbon-phenolic-in-air species, a CFD calculation of the Stardust re-entry at 71 km is presented. The code used for that purpose has been designed to take advantage of the nature of the problem and therefore remains very efficient when a high number of chemical species are involved. The CFD result demonstrates the need for such chemistry model when modeling the flow field around an ablative material. Modeling of the nonequilibrium radiation spectra is also presented, and compared to the experimental data obtained during Stardust re-entry by the *Echelle* instrument. The predicted emission from the CN lines compares quite well with the experimental results, demonstrating the validity of the current approach.

1. Introduction

The Thermal Protection System (TPS) of a re-entry vehicle is one of the key components of its design. The materials used for the TPS can be classified into two main categories: ablative materials, such as the ones used on the Apollo missions, and non-ablative materials, such as the ceramic tiles used on the Space Shuttle. The former can also be divided into two sub-categories: charring (also know as pyrolyzing) and non-charring ablators. The theory behind the use of ablators is quite simple: the energy absorbed by the removal of material from the surface is not used to heat the TPS, thus keeping the vehicle at a relatively "cold" temperature. In the case of charring ablators, the ablative material is a resin which fills the pores of a carbon matrix. Although the matrix may ablate, it usually does not, thus preserving the original geometry of the aerodynamic surface during re-entry.

In order to properly model the heating rates at the surface of the vehicle, the ablating boundary condition must take into account many phenomena: surface recession, wall temperature, blowing rates, gas composition, surface chemistry, etc. However, to account for the effects of the pyrolysis gas on the vehicle, the chemistry model of the flow field must include

the reactions associated with the presence of this gas. Because ablation coupling is becoming an increasingly important research topic [1–4], the development of an accurate, yet usable, chemistry model is of great importance. Models have been proposed in the past [5–7] but important reactions were not included, and some of the reaction rates were inappropriate or simply outdated.

Recently, a more complete model was proposed [8], which includes an extensive set of kinetic rates, taken from the combustion community. The model was reduced using 0-D sensitivity analysis over a parameter space relevant to the re-entry conditions that such a material would be exposed to. It was established that such a model was necessary to study carbon-phenolic TPS through a review of past models, which gave a wide range of results, especially when radiative heat transfer calculations were performed [9]. The reduced model was later integrated into the hypersonic Computational Fluid Dynamics (CFD) code LeMANS. Since the model is composed of 38 species and 158 reactions, the number of conservation equations to be solved significantly increases, as does the computation times. However, because LeMANS was parallelized efficiently with respect to the intrinsic characteristic of the problem, the code remains efficient, robust and fast, even in these conditions. As a test case, this paper presents results of the 71 km trajectory point of the Stardust return vehicle, and compares them with measurements of the experimental data obtained from the *Echelle* spectrometer.

2. LeMANS: an unstructured three-dimensional Navier-Stokes solver for hypersonic nonequilibrium aerothermodynamics

The hypersonic aerothermodynamic CFD code used to analyze the chemistry model is LeMANS, a finite volume Navier-Stokes solver currently being developed at The University of Michigan [10–13]. The code assumes that the translational and rotational energy modes of all species can be described by their respective temperatures T and T_r, as is the free electron temperature T_e. The vibrational energy mode and electronic energy mode of all species is however described by a single temperature, T_{ve} [14]. The viscous stresses are modeled assuming a Newtonian fluid, using Stokes' hypothesis, and the species mass diffusion fluxes are modeled using a modified version of Fick's law. Mixture transport properties are calculated using one of two models; the first uses Wilke's semi-empirical mixing rule with species viscosities calculated using Blottner's model and species thermal conductivities determined using Eucken's relation, and the other uses Gupta's mixing rule with species viscosities and thermal conductivities calculated using non-coulombic/coulombic collision cross section data. Heat fluxes are modeled according to Fourier's law for all energy modes. Finally, the source terms of the species conservation equations are modeled using a standard finite-rate chemistry model for reacting air in conjunction with Park's two-temperature model to account for thermal nonequilibrium effects on the reaction rates.

To account for the ablating TPS, a blowing boundary condition which solves the conservation of momentum at the wall and the mass balance is available in LeMANS [15]. The energy balance equation, which can be solved using the strongly coupled material response code MOPAR [16], is not required in the current analysis.

The code has the capability to handle meshes containing any mix of hexahedra, tetrahedra, prisms and pyramids in 3D, or triangles and quadrilaterals in 2D. Numerical fluxes between the cells are discretized using a modified Steger-Warming Flux Vector Splitting scheme, which has low dissipation and is appropriate to calculate boundary layers. A point or line implicit method is used to perform the time integration. The code has been extensively validated against experimental data, and has also been compared to other similar codes such as NASA Ames' DPLR [17] and NASA Langley's LAURA [18].

2.1. Implicit Line Solver

The system of equations used to numerically simulate hypersonic, chemically reacting viscous flows is very stiff. One of the options to overcome the time-step limitations in such a case is using implicit time integration. The developed code can use a point-implicit or a line-implicit method to solve the set of equations implicitly. The line implicit method has better convergence performance but it comes at the expenses of a more complicated algorithm. A line in the system of equations to be solved can be written as

$$A_i \Delta Q_i + \sum_j B_j \Delta Q_{nb} = R_i^n \tag{1}$$

where A and B contain the inviscid and viscous jacobians, R is the residual of the system of equations and ΔQ is the correction used in the time march. The summation in the last expression is over all j-th faces that form the i-th cell. Moreover, nb stands for the neighbor of the i-th cell that shares the j-th face. Details of the formulation can be obtained in Ref. [11]. When using unstructured grids, Eq. 1 is a sparse matrix without any structure. Considering the mesh shown in Fig. 1a), the corresponding matrix form of Eq. 1 is shown in Fig. 2a). There are many algorithms available for efficient solution of sparse linear systems. Such algorithms rely heavily on general mathematical properties of matrices to solve the system. These algorithms, however, do not take into account some flow characteristics that can simplify the system. For instance, flow gradients will be stronger in the direction normal to the body according to boundary layer theory. It was shown [19] that solving the system of equations exactly in the normal direction for structured grids and relaxing the system in the other directions was a good option to parallelize an implicit code.

The idea of solving the linear system originated by an implicit method using special directions in unstructured grids is not new [20, 21]. The first step in such a method is to define the special directions that will be used. In this work, such directions are called lines that are grown from the body surface by a simple algorithm that chooses the next cell such that the line stays nearly normal to the body. Cells that are left over are grouped together and handled by a point implicit algorithm. The lines formed from the mesh in Fig. 1a) are indicated in Fig. 1b). That figure also shows a renumbering of the cells that will be shown to facilitate the solution of the linear system. The renumbering of the cells is never carried out in the code. Instead, an array keeps track of the relation between the two cell numbering systems.

Using the numbering for the cells provided in Fig. 1b), the sparse system is greatly simplified as can be observed in Fig. 2b). The matrix is still sparse, but one can see a tridiagonal structure embedded in the matrix. In order to take advantage of the tridiagonal structure, an iterative process is assembled. All the terms off the tridiagonal part of the matrix are moved to the right hand side of the equation. By doing that, the iterative process is now of the form depicted in Fig. 3. The last three lines of the system represent the three cells left over from the line finding procedure. Those cells corrections are calculated using a simple point implicit method which is naturally integrated in the tridiagonal solver. Due to its diagonal characteristic, the system is very simple to solve. Assuming that $\Delta Q(n+1,0) = 0$, $\Delta Q(n+1,1)$ is obtained by solving a simple tridiagonal system of equations. The next step requires a multiplication of the sparse matrix on the right hand side by the newly calculated $\Delta Q(n+1,1)$. That multiplication is straightforward when using the face based data structure of the mesh and the mesh numbering. The result of that multiplication is mapped to the linear system numbering and a new right hand side is fed to the tridiagonal solver. Following Ref. [19], four iterations are taken in the iterative process. The code starts running with a very small CFL number which is increased to a maximum value of 10 when using a second order scheme or 1000 when using a first order scheme.

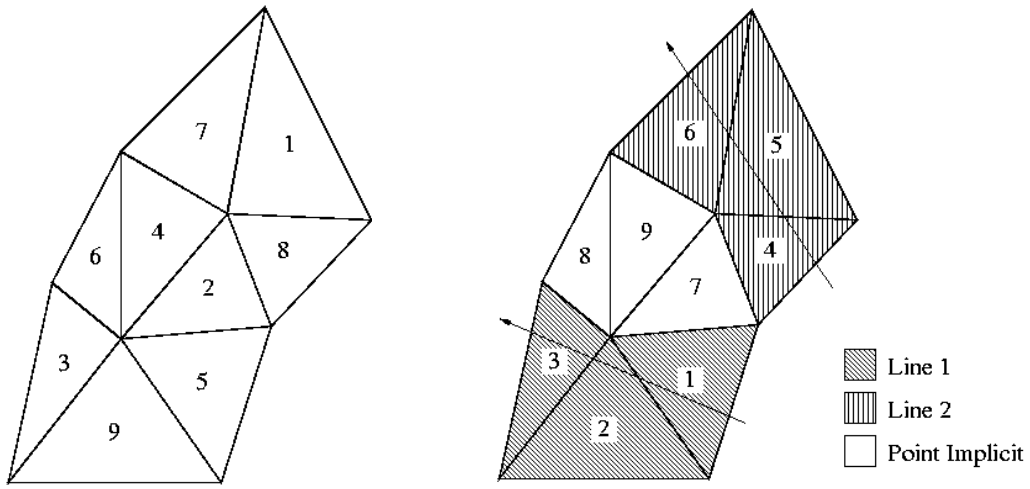

(a) Mesh (b) Linear system

Figure 1. Distinct numbering used in the code

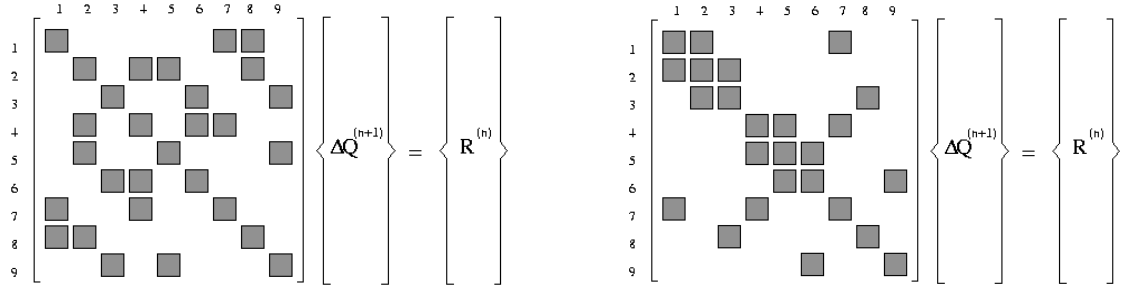

(a) Original numbering (b) Renumbered

Figure 2. Typical linear systems for the unstructured grids of Fig. 1

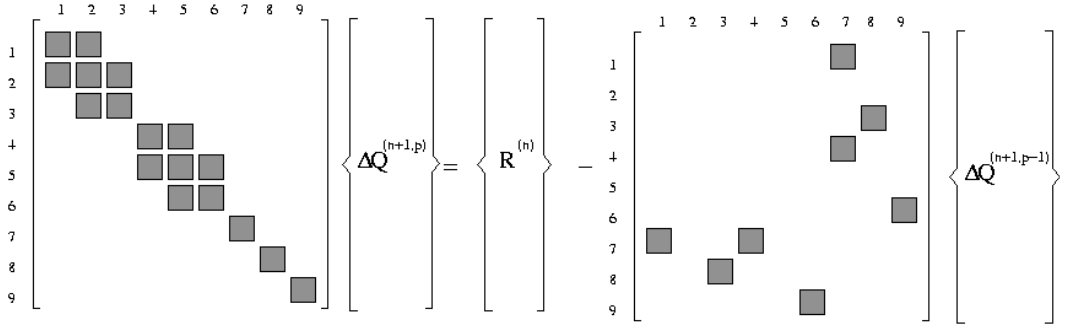

Figure 3. Iterative solution of linear system

2.2. Parallel Processing

The code developed in this work takes full advantage of modern parallel machines by dividing the computational work among many processors. This task is accomplished using METIS [22] to partition the mesh between the processors and MPI to communicate necessary information from one processor to another. METIS uses graph theory to partition unstructured grids minimizing the amount of inter-processor communication. Each node in the graph corresponds to a cell in the mesh. Each edge in the graph connecting two nodes corresponds to the face shared by the cells represented by the two nodes. A partition generated in this way usually is not optimal for a line implicit solver because most of the lines are significantly shortened. In order to avoid such a problem, the graph is modified so that each node in fact corresponds to a line and each edge corresponds to all the faces connecting one line to another. The weights of the nodes in the graph are set to the number of cells that form the line and the weight of each edge is equal to the number of faces connecting each line so that the load balancing of the partitions is not reduced. The implemented algorithm is highly effective as can be observed in Fig. 4 which shows the partitions for a hybrid unstructured grid and for a structured like grid.

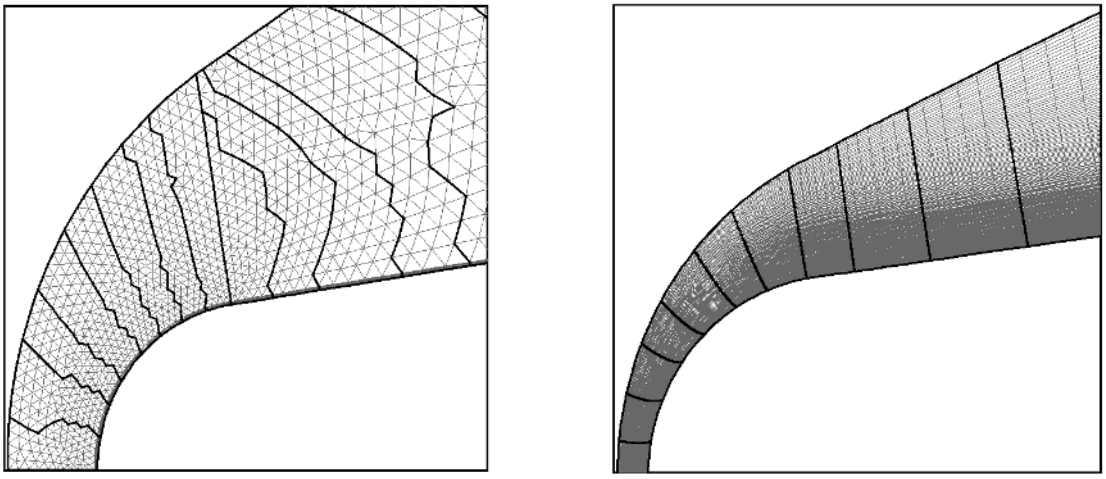

(a) Triangular grid (b) Quadrilateral grid

Figure 4. Mesh partitioning

2.3. Chemistry model

The chemistry model used in this analysis has been developed and optimized for vehicles equipped with ablative heat shields composed of PICA, re-entering in a N_2-O_2 atmosphere [8, 23]. The species and reaction mechanisms used in the model were carefully selected using a material response analysis. The corresponding kinetic chemistry rates were taken from the GRI-MECH model, and then reduced using a sensitivity analysis [8, 9, 23]. The reduced model contains 38 species and 158 reaction rates. The selected species can be grouped into three categories; the air species:

$$N_2,\ O_2,\ NO,\ N,\ O,\ N_2^+,\ O_2^+,\ NO^+,\ N^+,\ O^+,\ e$$

the surface species:

$$H_2,\ CO,\ CH_4,\ H_2O,\ CO_2,\ OH,\ C_2H_2,\ HCN,\ C_2H,\ C_3,\ CN$$

and the reacting species:

$$H,\ NH,\ HO_2,\ H_2O_2,\ HCO,\ C,\ C_2,\ CH,\ CH_2,\ CH_3,\ NCO,\ HNO,\ CO^+,\ CN^+,\ C^+,\ H^+$$

The reaction mechanisms and kinetics rates are listed in Ref. [9]. The model has been validated with multiple zero-dimensional simulations performed using the CHEMKIN [24] package, and compared to available experimental data that are representative of an ablative boundary layer during hypersonic re-entry [8].

3. Test-case: Stardust re-entry vehicle at 71 km

3.1. Problem description

In order to evaluate and validate the model used in LeMANS, the forebody of the Stardust return capsule is modeled at the 71 km trajectory point [25]. This re-entry point is chosen because it is well into the continuum region where the Navier-Stokes equations are valid, and spectral emission data obtained by the *Echelle* instrument is available. The geometry and mesh are presented in Fig. 5 and the flow and surface parameters are given in Tables 1 and 2, respectively. To complete the chemistry model described earlier, Gibb's Free Energy is used to calculate the equilibrium constants needed for the backward reaction rates, and the transport properties are calculated from Lennard-Jones potentials, using CHEMKIN [24], to produce temperature dependent viscosity curve fits for each species.

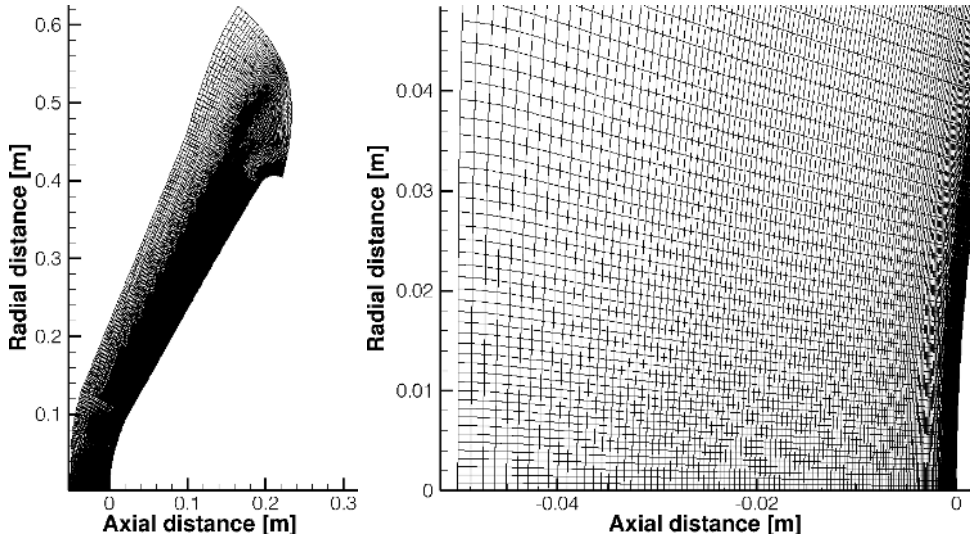

(a) Geometry and overall mesh (b) Stagnation region mesh

Figure 5. Geometry and mesh of the Stardust re-entry capsule, used for the chemistry model comparison

The values used for the surface temperature, blowing rates and gas composition are obtained with an uncoupled approach, using a combination of three NASA software tools. First, the aeroheating environment is calculated using DPLR [26]. The heat transfer coefficient, the surface pressure and the freestream enthalpy are then used in the material response code, FIAT [27]. The pressure and the non-dimensionalized ablation rate, B'_g and B'_c, values predicted by FIAT are then extracted and input to the Multicomponent Ablation Thermochemistry (MAT) code [28]. When given this information, MAT calculates back from the B' tables the species mole fractions according to JANNAF information corresponding to the wall temperature predicted by

Table 1. Free stream conditions for the 71 km trajectory point of the Stardust re-entry vehicle

Altitude [km]	U_∞ [km/s]	T_∞ [K]	ρ_∞ [kg/m^3]	Y_{N_2}	Y_{O_2}	Kn
71.2	12.1	222.	5.55×10^{-4}	0.763	0.237	0.00145

Table 2. Wall condition at the stagnation point for the 71 km trajectory point of the Stardust re-entry vehicle

T_w [K]	$\dot{m}_w$ [kg/m^2/s]	Y_{N_2}	Y_{CO}	Y_{H_2}	Y_{H_2O}
3240.	0.0453	6.75×10^{-1}	1.23×10^{-1}	5.76×10^{-3}	5.23×10^{-2}

Y_{OH}	Y_O	Y_{CO_2}	Y_{NO}	Y_{O_2}	Y_N
3.30×10^{-2}	3.68×10^{-2}	2.70×10^{-2}	1.74×10^{-2}	2.99×10^{-2}	0.00

FIAT. This procedure therefore provides input values for blowing rates, wall temperature and equilibrium species composition. It is to be noted that the equilibrium condition is computed while accounting for the boundary layer edge gas (air) and the surface material (carbon), and therefore accounts for surface ablation. The downside of this procedure is that mass is introduced at the surface as the boundary layer edge gas and is considered to be injected at the surface. However, at this altitude the added mass is negligible, since the blowing rate is less than 1% of the freestream mass flux.

The values obtained through this procedure are only calculated at the stagnation point and are expected to be significantly lower elsewhere on the forebody of the vehicle. To reflect this, a temperature profile is obtained using a fully radiative equilibrium boundary condition at the wall, without ablation. The surface temperature profile is then normalized and re-applied for the ablating wall simulation, multiplied by the surface temperature at the stagnation point that is listed in Table 2. This method has been proven to give a good estimate of the surface conditions [25]. For the blowing rate, a linear relation between the temperature and the mass flux is derived using the second and third columns of Table 2, and applied proportionally using the normalized surface temperature profile.

3.2. Results – convective heat flux

The convective heat flux obtained with the ablative boundary condition, using the proposed chemistry model, is presented in Fig. 6. As expected, the heat flux is significantly reduced when compared to the radiative equilibrium heat flux, also presented in that figure. As can be seen in Fig. 7, most of the heat reduction comes in the form of the mass diffusion term. This is a different phenomenon than that observed at higher altitude [23], where the majority of the reduction in heat flux occurred through the translational-rotational term. A decrease of this latter term is still observed, of approximately the same magnitude as at the higher altitude trajectory point, but it is no longer the dominating factor. The reduction in the mass diffusion term is explained by the increased blowing rates which causes the mixing region to be thicker, thus reducing the species gradients near the wall. The reduction of the translational-rotational conduction term is caused by a slight modification of the temperature gradients, due to the fact

that the shock is pushed away from the surface by the blowing at the surface. Additionally, the change in boundary layer composition causes a modification of the thermal conductivity of the gas, which also acts to reduce this term.

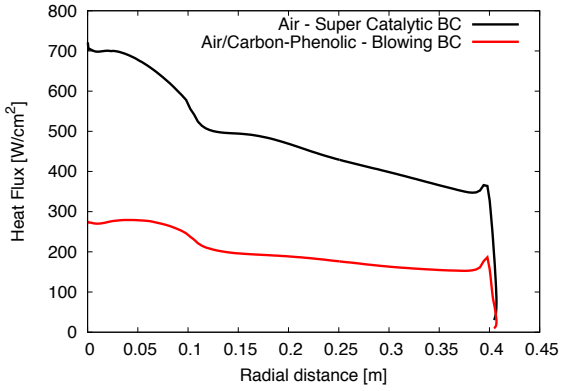

Figure 6. Heat fluxes at the surface of the Stardust re-entry vehicle at 42 s into re-entry (71 km), computed using an air-only chemistry model in the flow field with supercatalytic boundary conditions, and the carbon-phenolic-in-air chemistry model, with a blowing boundary condition

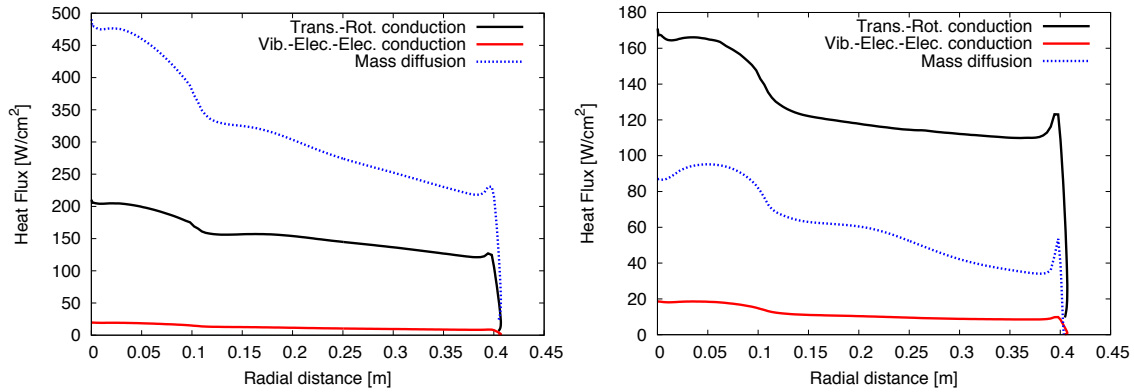

(a) Air-only chemistry; supercatalytic boundary condition

(b) Carbon-phenolic-in-air chemistry; blowing boundary condition

Figure 7. Individual heat flux components

3.3. Results – species concentrations

The species composition along the stagnation line is presented in Fig. 8. It is interesting to note in Fig. 8b) that most of the C-H blowing species (CO_2, H_2, OH and H_2O) are destroyed almost immediately once they enter the flow, although CO remains in high concentration. This species is important since it is itself a strong radiator, but more importantly, it is the main source of CN through the CO/CN exchange reaction, and CN is one of the strongest radiators at re-entry conditions. In Fig. 8c), it can be seen that most blowing species are transformed into atomic species (H and C), as they are present in high concentrations near the boundary. This figure also shows that CN is also present in great quantities. It is also interesting to note, in that same figure, that the concentration of HNO is relatively high near the shock; this species was neglected in past models [5–7]. Finally, Fig. 8d) presents the species which are not present in a significant concentration (species that had a number density less than the machine precision are not shown). Although it might be tempting to discard them, they remain important since

they start to appear in greater concentration at other re-entry conditions (i.e. other altitudes). The same calculations were performed for the other trajectory points, as presented in Ref. [8], and although some differences are noticeable, the general conclusions remain the same.

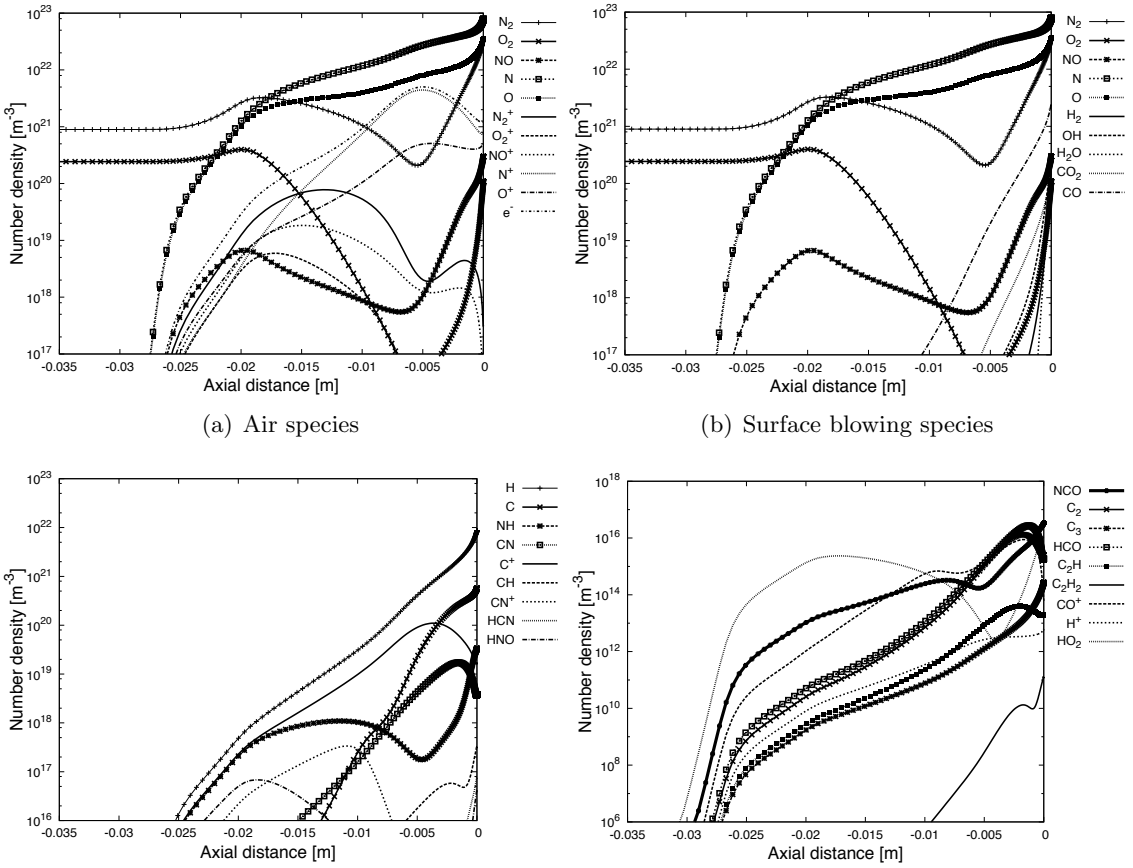

(a) Air species

(b) Surface blowing species

(c) High concentration species

(d) Low concentration species

Figure 8. Species concentrations along the stagnation line for the Stardust vehicle 42 s into re-entry (altitude of 71 km)

3.4. Results – radiative heat flux

Certain species present in the boundary layer are strong radiative emitters, and are expected to significantly contribute to the overall radiative heat flux at the surface. For the Stardust re-entry vehicle, the contribution of the radiative heat flux to the overall heat flux has been evaluated, at maximum intensity, to be approximately 10% [25].

A radiative emission calculation is performed using the flow field solution of the 42 s trajectory point (71 km), with the NEQAIR (version 99d) [29] non-equilibrium radiation code. Apart from the usual air species, radiative emission from the CN violet and CN red systems is included.

The stagnation line temperatures and species concentrations used as inputs to NEQAIR are presented in Fig. 9.Since the observation took place far away from Stardust, and the radiation is mostly emitted from the volumetric plasma in front of the vehicle and not from the surface, there is no need to account for the observation angle from which the data was acquired.

From Fig. 9b), it is interesting to note that CN^+ plays a more significant role in the determination of the species concentrations than was previously thought. It is created at the

cost of CN, and therefore reduces the CN concentration by up to two orders of magnitude in a region where the vibrational-electron-electronic temperature is high. The same cannot be said about CO^+, as nowhere in the flow is that molecule present in quantities that approach the concentration of CO.

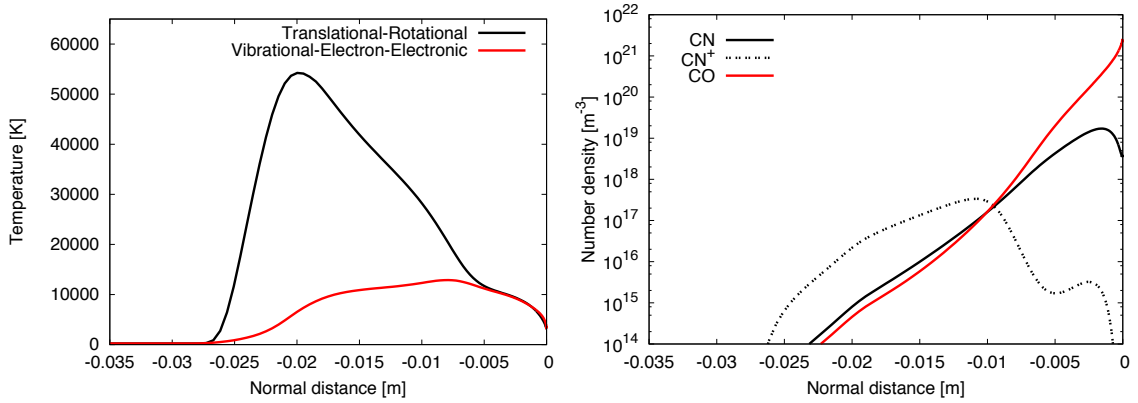

(a) Temperatures (b) Radiating species from ablation

Figure 9. Temperatures and CN/CO species concentrations along the stagnation line for the Stardust vehicle at 42 s into re-entry (71 km).

A comparison of the spectral emission from CN is presented in Fig. 10. It can be seen in that figure that the spectral computations match the *Echelle* data remarkably well, as the numerical results are within the same order of magnitude.

Finally, the radiative heat flux has also been computed for the test-case. The total radiative flux is approximately 1% of the convective heat flux, making it negligible at this trajectory point. What is more significant, however, is that a large portion (30-40%) of the radiative heat flux is generated by CN over the wavelength range of the *Echelle* instrument (about 360 to 890 nm), which further confirms the importance of properly modeling that particular species.

4. Conclusion

In an attempt to assess the importance of accounting for ablation species in the flow field, a new 38 species carbon/phenolic-in-air chemistry set was implemented in the hypersonic non-equilibrium CFD code LeMANS. Because of the way LeMANS has been parallelized, the code remains efficient, robust and fast, even with the increased number of equations to solve. As a test case, the Stardust vehicle at the 71 km trajectory point of its re-entry was used. This point was chosen because it is well into the continuum regime, and experimental data is available in the form of spectral radiative emission gathered by the *Echelle* instrument. As expected, the convective heat flux predicted using the carbon-phenolic-in-air chemistry model was significantly reduced relative to the prediction obtained using the equilibrium radiative boundary conditions. The species concentrations along the stagnation line were also presented and it was shown that at chemical equilibrium conditions, most species blown from the surface immediately react in the flow field and are transformed. These results clearly indicate the need to use an appropriate chemistry model in the flow field, and that the chemistry model should be significantly different than that used to model pyrolysis gas behavior inside the TPS. The flow field solution was also used to perform analysis of the CN radiative spectral emission using NEQAIR. The result compared remarkably well to the experimental data obtained by the *Echelle* instrument, and therefore provides increased confidence in the current approach.

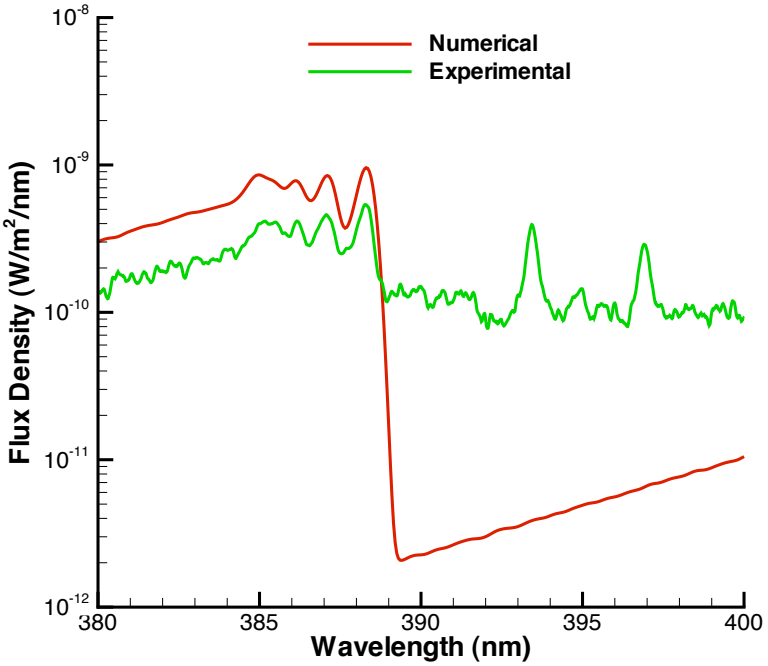

Figure 10. Comparison of the CN spectral line for the Stardust re-entry vehicle at 71 km

Acknowledgments
Financial support for this work was provided by NASA SBIR Phase-1 Award NNX10CC53P, NASA Prime Contract NNA04BC25C to ELORET Corporation and NASA Kentucky EPSCoR RIDG program. The authors would also like to thank Dr. Erin D. Farbar at the University of Michigan as well as Dr. Mike Wright, Dr. Ioana Cozmuta, Dr. David Hash, Dr. Nagi Mansour, Dr. Mike Barnhardt, Dr. Jean Lachaud and Dr. Tahir Gökçen from NASA Ames Research Center for numerous insightful discussions.

References

[1] Suzuki T, Sawada K, Yamada T and Inatani Y 2005 *Journal of Thermophysics and Heat Transfer* **19** 266–272

[2] Amar A J, Blackwell B F and Edward J R 2007 *39th AIAA Thermophysics Conference* AIAA-2007-4535 (Miami, FL)

[3] Milos F and Chen Y K 2008 *46th AIAA Aerospace Sciences Meeting and Exhibit* AIAA-2008-1223 (Reno, NV)

[4] Martin A and Boyd I D 2008 *40th AIAA Thermophysics Conference* AIAA-2008-3805 (Seattle, WA) p 20

[5] Park C, Jaffe R L and Partridge H 2001 *Journal of Thermophysics and Heat Transfer* **15** 76–90

[6] Suzuki K, Kubota H, Fujita K and Abe T 1997 *32nd AIAA Thermophysics Conference* AIAA-1997-2481

[7] Olynick D, Chen Y K and Tauber M E 1999 *Journal of Spacecraft and Rockets* **36** 442–462

[8] Martin A, Boyd I D, Cozmuta I and Wright M J 2010 *48th AIAA Aerospace Sciences Meeting and Exhibit* AIAA-2010-1175 (Orlando, FL)

[9] Martin A and Boyd I D 2010 *10th AIAA/ASME Joint Thermophysics and Heat Transfer Conference* AIAA-2010-4656 (Chicago, IL)

[10] Scalabrin L C and Boyd I D 2007 *39th AIAA Thermophysics Conference* AIAA-2007-4044 (Miami, FL)

[11] Scalabrin L C 2007 *Numerical Simulation of Weakly Ionized Hypersonic Flow Over Reentry Capsules.* Ph.D. thesis The University of Michigan Ann Arbor, MI

[12] Scalabrin L C and Boyd I D 2005 *38th AIAA Thermophysics Conference* AIAA-2005-5203 (Toronto, Ontario)

[13] Scalabrin L C and Boyd I D 2006 *9th AIAA/ASME Joint Thermophysics and Heat Transfer Conference* AIAA-2006-3773 (San Francisco, CA)

[14] Farbar E D, Boyd I D, Kim M and Martin A 2011 *42nd AIAA Thermophysics Conference* (Honolulu, HI)

[15] Martin A and Boyd I D 2010 *Journal of Thermophysics and Heat Transfer* **24**

[16] Martin A and Boyd I D 2009 *41th AIAA Thermophysics Conference* AIAA-2009-3597 (San Antonio, TX)

[17] Wright M J, Candler G V and Bose D 1998 *AIAA Journal* **36** 1603–1609

[18] Gnoffo P A 1989 *9th AIAA Computational Fluid Dynamics Conference* AIAA-1989-1972-CP (Buffalo, NY) pp 415–425

[19] Wright M J 1997 *A Family of Data-Parallel Relaxation Methods for the Navier-Stokes equations* Ph.D. thesis University of Minnesota Minneapolis, MN

[20] Venkatakrishnan V 1995 *VKI Lecture Series* VKI–LS–1995–02

[21] Nompelis I, Drayna T W and Candler G V 2005 *17th AIAA Computational Fluid Dynamics Conference* AIAA 2005-4867 (Toronto, ON)

[22] Karypis G and Kumar V 1998 *METIS: A Software Package for Partitioning Unstructured Graphs, Partitioning Meshes, and Computing Fill-Reducing Orderings of Sparse Matrices* Univeristy of Minnesota Minneapolis, MN

[23] Martin A and Boyd I D 2011 *49th AIAA Aerospace Sciences Meeting and Exhibit* AIAA 2011-143 (Orlando, FL)

[24] Kee R J, Rupley F M, Miller J A, Coltrin M E, Grcar J F, Meeks E, Moffat H K, Lutz A E, Dixon-Lewis G, Smooke M D, Warnatz J, Evans G H, Larson R S, Mitchell R E, Petzold L R, Reynolds W C, Caracotsios M, Stewart W E, Glarborg P, Wang C, McLellan C L, Adigun O, Houf W, Chou C P, Miller S F, Ho P, Young P D, Young D J, Hodgson D W, Petrova M V and Puduppakkam K V 2006 CHEMKIN, release 4.1

[25] Trumble K A, Cozmuta I, Sepka S and Jenniskens P 2008 *46th AIAA Aerospace Sciences Meeting and Exhibit* AIAA-2008-1201 (Reno, NV)

[26] NASA Ames Research Center *DPLR Package Users Guide* 3rd ed

[27] Chen Y K and Milos F S 1999 *Journal of Spacecraft and Rockets* **36** 475–483

[28] Milos F S and Chen Y K 1997 *35th Aerospace Sciences Meeting and Exhibit* AIAA-1997-141 (Reno, NV)

[29] Whiting E E, Park C, Liu Y, Arnold J O and Paterson J A 1996 NEQAIR96, nonequilibrium and equilibrium radiative transport and spectra program: User's manual Reference Publication 1389 NASA